Heliyon 9 (2023) e16699

Contents lists available at ScienceDirect

Heliyon

journal homepage: www.cell.com/heliyon

Parameters optimization of Fe_3O_4 NPs synthesis by *Tamarindus indica* leaf extract possessing both peroxidase as well as excellent dye removal activity

Md Rajibul Akanda *, Md Al-amin, Masrifa Akter Mele, Zunayed Mahmud Shuva, Md Billal Hossain, Taohedul Islam, Md Mehedi Hasan, Umme Habiba Ema

Department of Chemistry, Jagannath University, Dhaka, 1100, Bangladesh

A R T I C L E I N F O

Keywords:
Fe_3O_4 nanoparticle
Tamarindus indica leaf Extract
Peroxidase activity
Dye removal activity
Green synthesis

A B S T R A C T

This study reports optimized conditions for the green synthesis of iron (II,III) oxide nanoparticles (Fe_3O_4 NPs) from *Tamarindus indica (T. indica)* leaf extract. The synthetic parameters like concentration of leaf extract, solvent system, buffer, electrolyte, pH, and time were optimized for Fe_3O_4 NPs synthesis. Fe_3O_4 NPs were obtained from the synthesis protocol by measuring size (80 ± 3 nm approx.), characteristics color changes, and an absorption peak between 270 nm and 280 nm using a UV–visible spectrophotometer, scanning electron microscope (SEM), and an energy dispersive X-ray spectrometer (EDS) study. Peroxidase activity was tested with 3,3,5,5–Tetramethylbenzidine (TMB) oxidation in the presence of hydrogen peroxide and dye removal activity was tested with malachite green (MG). The results indicated that the successful synthesis of Fe_3O_4 nanoparticles using aqueous leaf extract of *T. indica* is a practical alternative for biomedical applications due to its potent peroxidase activity and high dye removal capacity (about 93% with UV light and 55% with room light).

1. Introduction

Recent times have seen a lot of interest in green nanotechnologies for iron-oxide nanoparticle synthesis due to their applications in biomedicine, cosmetics, bioremediation, diagnostics, and materials engineering [1–5]. The unique properties like biocompatibility, biodegradability, low toxicity, small size, and peroxidase activity are responsible for its high demand in the biomedical sectors [6–11]. In addition to green nanotechnology, a number of other technologies like physical, chemical, biological, and mixed methods are being used to synthesize iron-oxide nanoparticles [12–15]. Moreover, the specific method of nanosynthesis can only enhance specific properties [16]. In this article, we limited our focus to green nanotechnologies for the synthesis of iron-oxide nanoparticles having prominent catalytic activities.

Nanoparticles of iron-oxide can have different compositions, such as iron (II) oxide nanoparticles (FeO NPs), iron (III) oxide nanoparticles (Fe_2O_3 NPs), and iron (II,III) oxide nanoparticles (Fe_3O_4 NPs) [17–19]. Among those, Fe_3O_4 NPs are our focus of interest because of their excellent paramagnetism, high coercivity [20], low Curie temperature [21–24], extremely low toxicity, and excellent biocompatibility [25]. With all of these properties, Fe_3O_4 NPs can be used in a variety of biomedical applications, including cell

* Corresponding author.
E-mail addresses: rhakanda@gmail.com, rhakanda@chem.jnu.ac.bd (M.R. Akanda).

https://doi.org/10.1016/j.heliyon.2023.e16699
Received 8 February 2023; Received in revised form 23 May 2023; Accepted 24 May 2023
Available online 27 May 2023
2405-8440/© 2023 The Authors. Published by Elsevier Ltd. This is an open access article under the CC BY-NC-ND license (http://creativecommons.org/licenses/by-nc-nd/4.0/).

therapy [26], drug delivery [27], photothermal effect [28], tissue engineering [29], regenerative medicine [30], hyperthermia [31], diagnosis [32] and imaging [33]. Moreover, because of its capability to facilitate the cellular and molecular level of biological interactions, Fe_3O_4 NPs are being considered as successful contrast agents for magnetic resonance imaging (MRI) in theranostics and nanomedicines [34], Fe_3O_4 NPs are well known for their unanimous photocatalytic and photo-oxidizing capacities. Inspired by the recent success in the green synthesis of copper (II) oxide nanoparticles [35,36] possessing excellent catalytic activity, we are interested to synthesize Fe_3O_4 NPs by novel green reductant and evaluate its catalytic activity.

Number of green plants such as *Lagenaria siceraria* [37], *Euphorbia herita* [38], *Phyllanthus niruri* [39], *Gracilaria edulis* [40], *Zanthoxylum armatum* [41], *Mikania mikrantha* [42], *Andean blackberry* [43], seaweed (*Colpomenia sinuosa* and *Pterocladia capillacea*) [44], *Mimosa pudica* [45], soyabean sprouts [46], *Garcinia mangostana* [47], *Morinda morindoides* [48], Ridge gourd [49], *Chromolaena odorata* [50], Seaweed (*Kappaphycus alvarezii*) [51], *Graptophyllum pictum* [52], plantain [53], RS Lichen [54], Gram bean [55], *Rhus coriaria* [56], *Couroupita guianensis Aubl* [57], were found to be used for the successful synthesis of Fe_3O_4 NPs. *Tamarindus indica* (*T. indica*) has not used for Fe_3O_4 NPs synthesis till now.

T. indica is a well-known plant for its medicinal value. Different parts of *T. indica* such as seeds, roots, bark, leaves, and fruits are used in traditional Indian and African medicine. It is usually prescribed for treating constipation and liver problems, pain and inflammation of joints, diarrhea and dysentery, bacterial infections, and parasitic infestations. It contains plenty of essential amino acids, phytochemicals, and vitamins and hence possesses pharmacological activity like antimicrobial, antioxidant, antidiabetic, hypoglycaemic, cholesterolemic, hypolipidemic, antihepatotoxic, and anti-inflammatory. It is expected that with the support of modern technology, it could be used as evidence-based medicine for many health problems [58]. The rich content of polyphenol in *T. indica* motivates us to evaluate its efficiency in Fe_3O_4 NPs synthesis for the first time. It is expected that the novel use of *T. indica* leaves extract and optimization of the Fe_3O_4 NPs synthesis procedure will produce NPs with prominent catalytic activity.

In the present study, *T. indica* leaf extract has been considered as a green reductant, and iron (III) chloride ($FeCl_3$) as a precursor. The leaf extract is not only a reductant but also a nanoparticle stabilizer. The leaf extract obtained in distilled water was evaluated for the synthesis of Fe_3O_4 NPs. Furthermore, the effects of the type of solvent system, type of buffer, its concentration, its electrolyte concentration, and concentration of peel extract on Fe_3O_4 NPs synthesis were evaluated thoroughly. Optimal conditions were used to synthesize Fe_3O_4 nanoparticles that exhibited potent peroxidase activity and excellent dye removal capability.

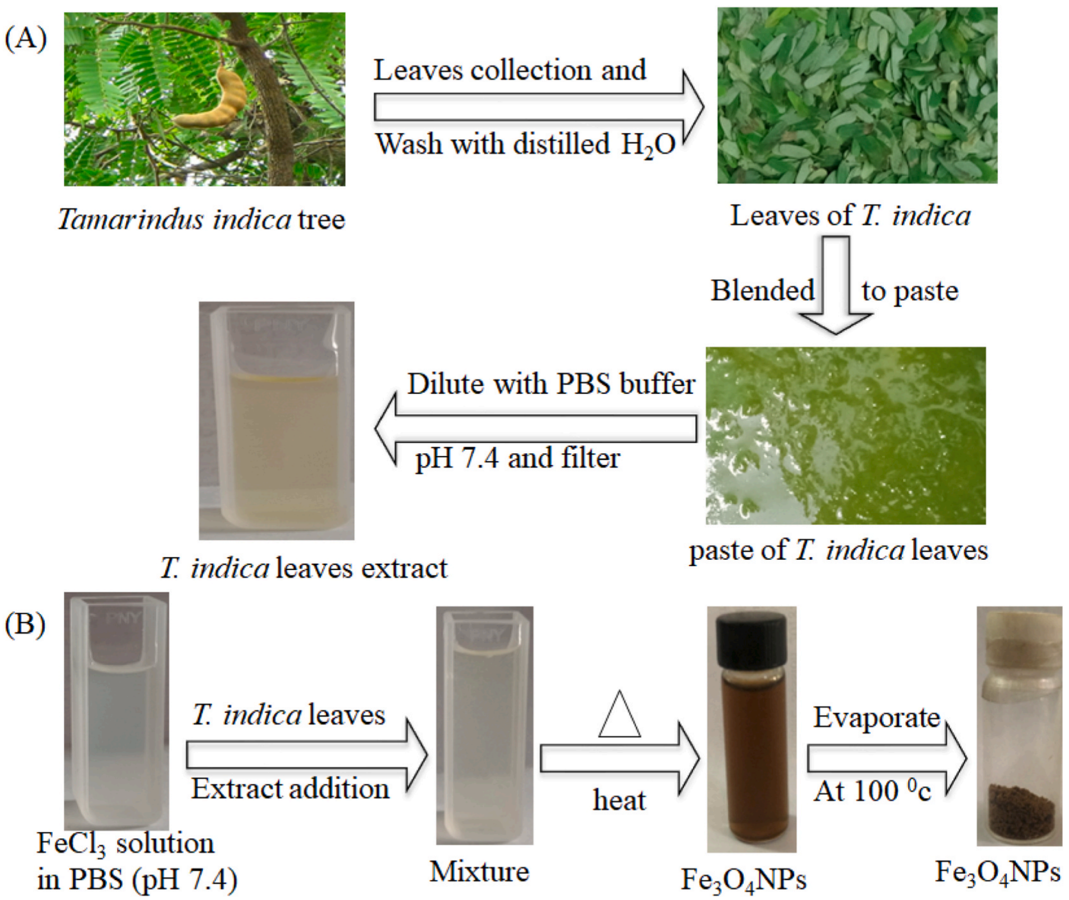

Scheme 1. Schematic representation for the (A) preparation of *T. indica* leaf extract and (B) synthesis of Fe_3O_4 NPs from *T. indica* leaf extract.

2. Experimental

2.1. Materials

T. Indica leaves were collected from the Bolda garden, Dhaka, Bangladesh. Iron (III) chloride ($FeCl_3$), aluminium chloride ($AlCl_3$), sodium chloride (NaCl), potassium chloride (KCl), sodium hydroxide pellets, hydrochloric acid (HCl), Sulphuric acid, 3,3,5,5 –Tetramethylbenzidine (TMB), hydrogen peroxide (H_2O_2), and Malachite green were obtained from Sigma-Aldrich (USA). The double-ring filter paper was from Hangzhou Xinhua Paper Industry Co. Ltd. The falcon tubes (50 mL and 25 mL) were purchased from Korea. Disodium mono hydrogen phosphate was purchased from Duksan Pure Chemicals Korea. Monosodium dihydrogen phosphate was obtained from Scharlab S. L. Spain. Distilled water was used throughout the reactions. All glassware was cleaned with dilute nitric acid (HNO_3), and distilled water, and dried in the oven.

2.2. Instrumentation

The double-beam spectrophotometer (model: UV-1800) was used for taking UV data. Attenuated Total Reflectance (ATR) (model: QATR-S) was used for ATR study. Magnetic stirrer with hot plate (model LMS-1003) was for stirring and controlling temperature, distilled water plant (model: CE-2) was used for preparing distilled water. A scanning electron microscope (SEM) (model JSM-7600 F) and an energy dispersive X-ray spectrometer (EDS) (model (SUPRA 55)-CARL ZEISS) was used for characterizing nanoparticles.

2.3. Preparation of T. indica leaf extract

T. indica, locally referred to as "tetul," and its leaves were collected from the Boldha botanical garden in Dhaka. The leaves were washed thoroughly with distilled water and dried at ambient temperature for a few hours. The dried leaves were blended into a paste. A 10 g paste was then diluted with 20 mL of 100 mM phosphate buffer saline (PBS) buffer pH 7.4 and left to stir for 30 min with a magnetic stirrer. For further experiments, the solution was filtered through double-ring filter paper and stored at 4 °C. The complete extraction procedure is schematically shown in Scheme 1(A).

2.4. Synthesis of Fe_3O_4 NPs using T. indica leaf extract

The filtered *T. indica* leaves extract was used for Fe_3O_4 NPs synthesis using $FeCl_3$ as a precursor, where leaves extract function principally as a reducing agent. In doing so, a 0.01 M $FeCl_3$ solution was prepared in distilled H_2O in a beaker. 5 mL 0.01 M $FeCl_3$ solution was added to a falcon tube containing 10 mL distilled water. Then 3 mL 0.5 g/mL leaves extract in PBS buffer pH 7.4 and 10 mL 100 mM PBS buffer pH 7.4 was added to the mixture. So, the final concentration of $FeCl_3$ was calculated to be 0.0017 M and the concentration of PBS buffer was 46 mM. Upon heating the solution at 60 °C, the reaction of synthesizing Fe_3O_4 NPs was completed within 30 min. In Scheme 1(B), the yellowish color of the $FeCl_3$ solution and leaves extract was converted to a dark brown color. Further heating to evaporate at 100 °C produces a dark brownish-colored solid mass of Fe_3O_4 NPs.

2.5. Phytochemical content in T. indica leaf extract

The phytochemical content of the leaf extract prepared according to the Scheme was then investigated. Phenolic derivatives, flavonoids, and tannins are considered potent phytochemicals responsible for nano synthesis. The total phenolic derivatives content in *T. indica* leaf extract was determined by the slightly modified Folin–Ciocalteu methodology [59]. Briefly, water solutions of 2–100 μg/mL of standard gallic acid were prepared. 1 mL of leaf extract (1 mg/mL) or 1 mL of standard solution was added to 1 mL of distilled water. 1 mL of 10% Follin–Cicocalteu's (F–C) reagent and 1 M sodium carbonate solution were both added to the mixture in a UV cell. The incubation period for the reaction was 60 min at room temperature and in the dark. A single-beam UV spectrophotometer was used to measure absorbance at 700 nm using distilled water as a blank. Polyphenol content was expressed as μg Gallic Acid Equivalents (GAE) per mg of plant material. The $AlCl_3$ colorimetric assay (with some modifications) [60] was used for total flavonoid content determination. Briefly, as 2–100 μg/mL quercetin standard solutions were prepared in 80% ethanol. 1 mL of extract (1 mg/mL) or standard solution was added to 200 μl of 10% $AlCl_3$ solution and followed by 3 mL of 95% ethanol. 0.2 mL of 1 M sodium acetate was added to the mixture in a UV cell. The incubation period for this reaction was 60 min in room temperature and in a dark environment. Single beam UV spectrophotometer was used to measure the absorbance at 415 nm where 80% ethanol was used as a blank. Total flavonoid contents were expressed as μg Quercetin Equivalents (QE) per mg of plant material. Slightly modified Sun et al. Methodology [61] was used to determine condensed tannins. Briefly, a 1 mL methanolic solution of extracts (1 mg/mL) was added to the mixture of 3 mL methanolic solution of 4% vanillin and 1.5 mL of concentrated HCl in a UV cell. Single beam absorbance was measured after 15 min of incubation of the reaction at 500 nm where methanol was used as a blank. The total condensed tannins are expressed as μg Quercetin Equivalents (QE) per mg of plant material.

2.6. Plausible mechanism for the formation of Fe_3O_4 NPs from its precursors

Although the exact mechanism for the formation of Fe_3O_4 NPs is not known but with the support of Z. Kozakova et al. [62], we are thinking our synthesized nanoparticles might follow the below mechanism as illustrated in equations (1)–(6) respectively. In this study, Fe(III) salt was considered as precursor and its hydroxide precipitate proceeds according to equation (1).

$$Fe^{3+} + 3OH^{-} \leftrightarrow Fe(OH)_3 \tag{1}$$

There is a possibility of formation of Fe_2O_3 particles according to equation (2).

$$2\ Fe(OH)_3 \leftrightarrow Fe_2O_3 + 3H_2O \tag{2}$$

But in presence of mild reducing agent (e.g. phenolic derivatives) and heat, Fe(II) may appear in the system as follows.

Such as phenolic derivatives (ROH) can undergo dehydration under heating condition and the so-formed phenolic aldehyde (RCHO) [63] derivatives which reduces Fe(III) to Fe(II) and gives ferrous hydroxide in the form of a green colloid according to equations (3)–(5).

$$2ROH \rightarrow^{\Delta} 2RCHO + 2H2O \tag{3}$$

$$2R\text{–}CHO + 2Fe^{3+} \leftrightarrow R\text{-}CO\text{–}CO\text{-}R + 2Fe^{2+} + 2H^{+} \tag{4}$$

$$Fe^{2+} + 2OH^{-} \leftrightarrow Fe(OH)_2 \tag{5}$$

Finally, both +2 and + 3 oxidation states of iron coexist in the solution mixture, thus resulting magnetite formation according to equation (6).

$$2Fe(OH)_3 + Fe(OH)_2 \leftrightarrow Fe_3O_4 + 4H_2O \tag{6}$$

2.7. Peroxidase activity experiment with Fe_3O_4 NPs

The Fe_3O_4 NPs could catalytically oxidize peroxidase substrates in company with H_2O_2, exhibiting a peroxidase-like activity as first reported by the Yan group [64]. In this work, the peroxidase-like activities of the green synthesized Fe_3O_4 NPs were evaluated by TMB oxidation, a peroxidase chromogenic substrate. Peroxidase activity experiments were performed in a tube containing 0.00208 M TMB solution in acetate buffer pH 4.5, 0.1 M H_2O_2, and 0.00025 M Fe_3O_4 NPs solution. UV-VIS spectrophotometer was used to evaluate the peroxidase activity, such as observed for the commonly used natural enzyme horseradish peroxidase (HRP) [65]. Due to high catalytic activity, TMB becomes fully oxidized to di-imine showing a yellow-colored complex. This method results in a measurement of absorbance at 450 nm with $\lambda_{max} = 450$ nm.

2.8. Dye removal experiment with Fe_3O_4 NPs

Dye removal experiments were performed in 50 mL of 10 mg/L of Malachite green (MG) dye solution in 250 mL Erlenmeyer flask at room temperature (25 ± 1 °C) using an orbital shaker. The shaking speed used was 200 rpm. The adsorbent dose (Fe_3O_4 NPs) was 1 mg/mL. Mixing time was determined to be 120 min. Finally, the removal efficiency was measured under room light and UV light respectively but not under sunlight as it is difficult to control the similar intensity of the sunlight over period of days. UV-VIS spectrophotometer was used to quantify the dye absorbance which ultimately result its concentration. Removal (%) of dyes was quantified considering the absorbance (at $\lambda_{max} = 600$ nm) using the following equations [66]:

$$\eta = \frac{C0 - Ct}{C0} x100\% \tag{7}$$

where η is the rate of removal of MG in terms of percentage, Co is the initial concentration of MG solution, and Ct is the concentration of the MG dyes at time t.

3. Result and discussion

3.1. Total phenolic, flavonoid, and tannin content in leaf extract

In the extract solution, the total phenolic derivatives or polyphenol content was measured by measuring its absorbance, which was found to be 2.4332 (data not shown). The absorption of the different concentrations of standard gallic acid solution 2, 30, 50, 70, and 100 μg/mL was used to prepare a calibration plot in Figure-SM-1 in the supplementary material. The analysis of the calibration curve shows that the slope and intercept were 0.01796 and −0.0766 respectively. The total phenolic derivatives content was calculated to be about 139.74 μg/mL GAE per mg of plant material.

The absorbance of the total flavonoid content and condensed tannin content was calculated to be 3.7194 and 0.2235 respectively (data not shown). The absorption of the different concentrations of standard quercetin solution 2, 30, 50, 70, and 100 μg/mL was used to prepare a calibration plot in Figure-SM-2 in the supplementary material. The analysis of the calibration curve shows that the slope and intercept were 0.1557 and −0.1025 respectively. The total flavonoid content and total condensed tannin content were calculated to be about 24.546 μg/mL and 2.093 μg/mL QE per mg of plant material respectively.

As described above, the formation of Fe_3O_4 NPs is largely attributed to the high concentration of total phenolic derivatives.

3.2. Confirmation of Fe_3O_4 NPs and optimization of leaf extract concentration impact

The synthesis of Fe_3O_4 NPs was confirmed through UV–visible spectroscopic studies as depicted in Figure-1. As can be seen in Figure-1A, the peak of Fe_3O_4 nanoparticles appears in the green curve within 250–350 nm [67], whereas a similar peak does not appear for $FeCl_3$ in the red curve and for leaves extract in the blue curve. Moreover, Figure-1B shows a linear dependence of absorbance on the concentration of leaf extract. Besides, the existence of a sharp peak indicates a uniform and well-stabilized condition. This study determined the ideal concentration of leaf extract to be 0.0536 g/mL as too high a concentration of extract may have a negative effect on nanoparticle activity.

3.3. Optimization of solvent system, buffer, pH, electrolyte and time for Fe_3O_4 NPs synthesis

As NPs synthesis is greatly influenced by its synthetic parameters [68], optimization of some key parameters such as the impact of a solvent system, type of buffer, pH, and electrolytes concentration on Fe_3O_4 NPs synthesis was assessed in Figure-2. Firstly Fe_3O_4 NPs synthesis was evaluated considering water (red curve) and PBS buffer pH 7.4 (64 mM) (blue curve) as solvents in Figure-2(A). The buffer system as a solvent significantly enhances nanoparticle synthesis. Different types of buffer, such as carbonate (red curve), borate (blue curve), and PBS (green curve) all having pH 7.4 (64 mM), were investigated as depicted in Figure-2(B). The results indicate that the phosphate anions of the PBS buffer (pH 7.4) might have better solvation capability of the iron ions in solution which ultimately can significantly facilitate the synthesis of Fe_3O_4 nanoparticles. Based on a study of the pH of PBS buffer, pH 7.4 (blue curve) was found to be more favorable than acidic pH 2.0 (red curve) and basic pH 12 (blue curve) as depicted in Figure-2(C). Finally, the impact of the presence of 137 mM NaCl and 2.7 mM KCl as electrolytes in PBS buffer solution is also evaluated. As shown in Figure-2(D), the presence of an electrolyte (red curve) greatly supports the formation of Fe_3O_4 nanoparticles by maintaining the pH value (7.4 in this case) compared with its absence (blue curve). Moreover, it was found that 30 min reaction time was sufficient for the formation of Fe_3O_4 NPs as shown in Figure SM-3 of the supplementary material.

3.4. Characterization of the synthesized Fe_3O_4 NPs at optimum conditions

After the successful synthesis of Fe_3O_4 NPs under optimized conditions, it was subjected to complete characterization by SEM, EDS, attenuated total reflectance (ATR), and X-ray diffraction (XRD) studies respectively. Based on the SEM images of Figure-3, a cubic morphology was obtained as in Figure-3(A), though some aggregation of Fe_3O_4 NPs was also observed to produce 80 ± 3 nm sized nanoparticles (calculated by using scal bar of SEM instrument) as in Figure-3(B) visualized by 30000 times magnification of 100 nm scale bar.

According to the EDS study of Figure-4(A), the synthesized Fe_3O_4 nanoparticles are highly pure, consisting solely of iron and oxygen. In addition, the ATR study Figure-4(B) revealed that all of the peaks for functional groups of leaf extract were also found on the surface of synthesized NPs. It means that the NPs are stabilized by leaf extract functional groups. Importantly the presence of strong absorption bands between 580 and 630 cm^{-1} indicates the Fe–O bond of magnetite NPs [69,70] and finally, from the analysis of the XRD pattern of Figure-4(C), the presence of the diffraction peaks of 2θ corresponds to [C] due to presence of leaf extract on NPs surface and the [111, 220, 311, 400, 511, 440] planes confirms the cubic crystallinity of the magnetite Fe_3O_4 NPs compared with standard XRD peaks (JCPDS card, file No. 19–0629) [71]. In addition, the presence of sharp peaks confirms the crystalline nature of the synthesized NPs.

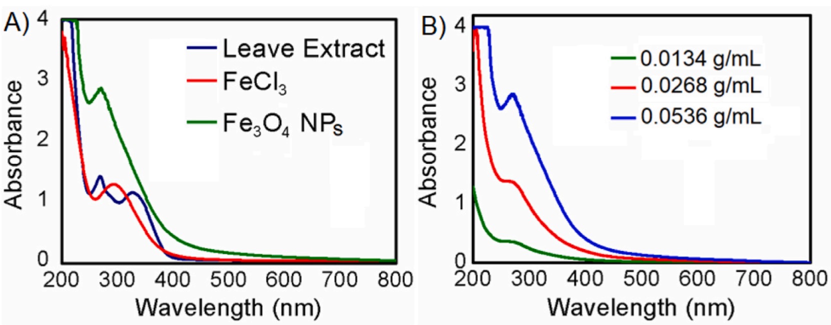

Fig. 1. UV–Visible spectra (A) of the synthesized Fe_3O_4 NPs (green curve), precursor 0.0017 M $FeCl_3$ (red curve) and 0.0536 g/mL leaves extract (blue curve) and (B) of the synthesized Fe_3O_4 NPs on 0.0536 g/mL (blue curve), 0.0268 g/mL (red curve) and 0.0134 g/mL (green curve) concentration of leaves extract in PBS buffer (46 mM) pH 7.4. (For interpretation of the references to color in this figure legend, the reader is referred to the Web version of this article.)

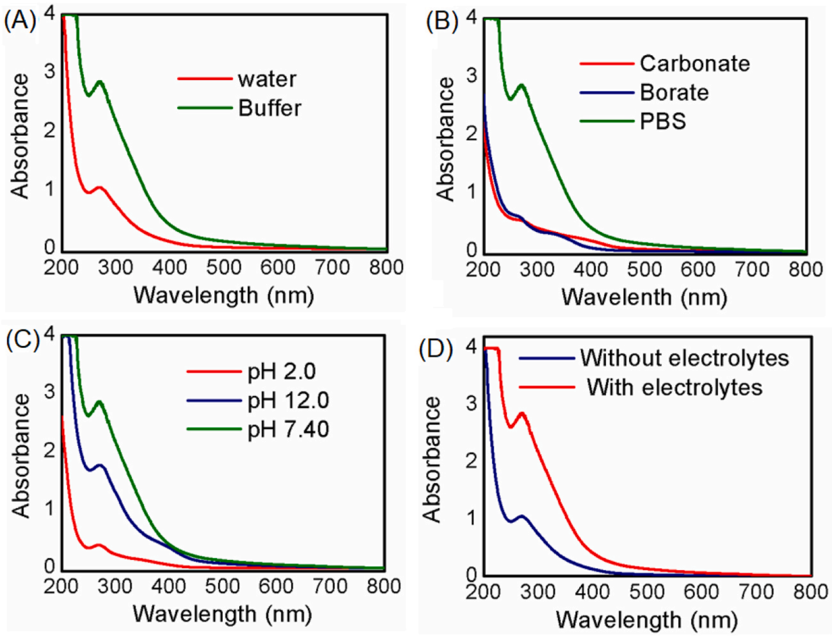

Fig. 2. UV–Visible spectra of the synthesized Fe_3O_4 NPs in (A) distilled water (red curve), PBS buffer (46 mM) pH 7.4 (green curve), (B) PBS buffer (green curve), Borate buffer (blue curve) and Carbonate buffer (red curve) (46 mM) pH 7.4, (C) PBS buffer (46 mM) pH 7.4 (green curve), pH 12.0 (blue curve) and pH 2.0 (red curve) and (D) PBS buffer pH 7.4 with 137 mM NaCl and 2.7 mM KCl as electrolyte (red curve), without electrolyte (blue curve) respectively. (For interpretation of the references to color in this figure legend, the reader is referred to the Web version of this article.)

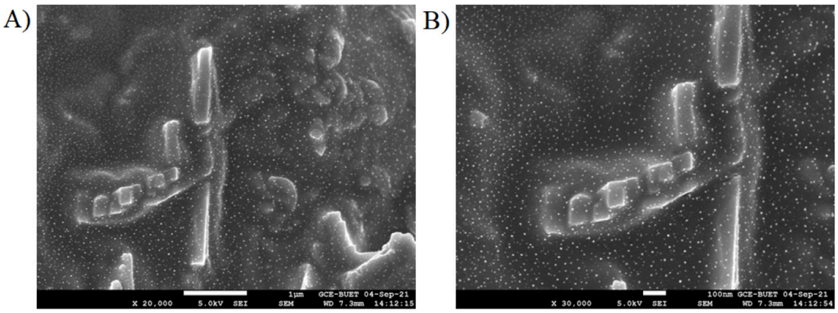

Fig. 3. SEM images of the synthesized Fe_3O_4 NPs as (A) 1 μm scal bar with ×20,000 magnification and (B) 100 nm scal bar with ×30,000 magnification in PBS buffer pH 7.4 with electrolyte.

3.5. *Peroxidase activity of Fe_3O_4 NPs*

Investigation of the peroxidase activity of the synthesized Fe_3O_4 NPs was carried out following the schematic depicted in Figure-5 (A). The color change from colorless to yellow indicated oxidation of the TMB solution in acetate buffer pH 4.5 to the di-iminium state of oxidized TMB, showing 2 electron transfer kinetics. As a result of this oxidation of TMB, a distinct peak was observed at 450 nm [72]. Investigation of Figure-5(B) revealed that TMB solution in acetate buffer pH 4.5 (red curve), H_2O_2 in distilled H_2O (blue curve), and a combination of both (green curve) did not show any peak at 450 nm. Therefore, oxidation of TMB is not possible with only H_2O_2. However, upon the addition of Fe_3O_4 NPs in PBS buffer (50 mM) pH 7.4 to the TMB and H_2O_2 mixture, a peak was observed at 450 nm. This study clearly confirmed the peroxidase catalytic activity of the synthesized Fe_3O_4 NPs.

3.6. *Dye removal activity of Fe_3O_4 NPs*

The synthesized Fe_3O_4 NPs were evaluated for dye removal activity. In doing so, we first checked the zero-point charge of Fe_3O_4 NPs in water system by investigating ΔpH (initial pH-final pH) Vs initial pH curve and it was found to be 6.8 as shown in figure-SM-4 of the supplementary materials. Dye removal activity was investigated in neutral condition of distilled water (pH 7.4). Therefore, malachite green (MG) [73], a cationic dye (Pka = 10.3) was used to determine dye removal capacity. At the neutral working pH of dye

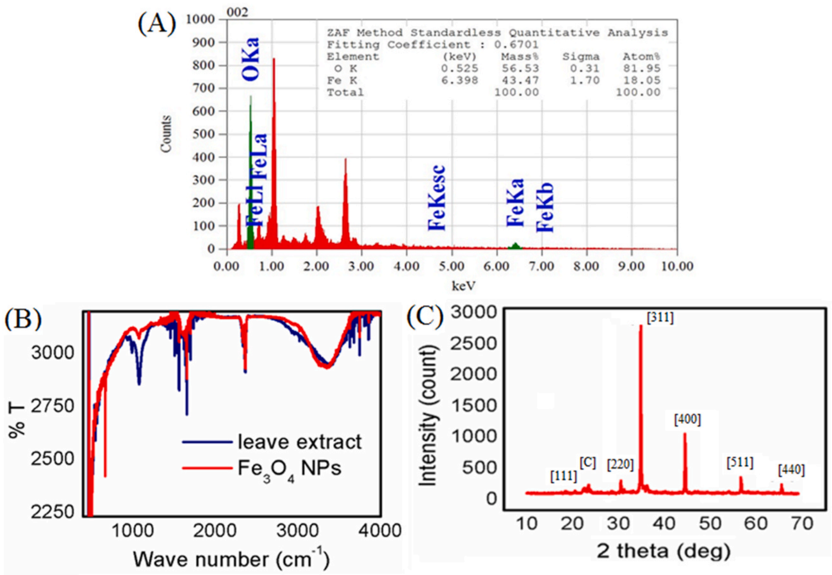

Fig. 4. (A) EDS, (B) ATR and (C) XRD spectra of the synthesized Fe_3O_4 NPs in PBS buffer pH 7.4 with electrolyte.

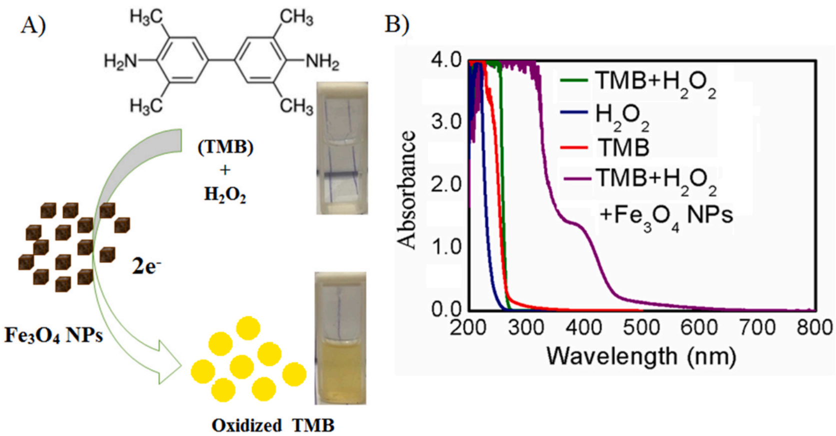

Fig. 5. (A) Schematic representation of TMB oxidation by H_2O_2 and Fe_3O_4 NPs as peroxidase enzyme and (B) UV–Visible spectra of the synthesized Fe_3O_4 NPs in PBS buffer (50 mM) pH 7.4 with 0.00208 M TMB (in acetate buffer pH 4.5), and 0.1 M H_2O_2.

solution the Fe_3O_4 NPs will be anionic in nature and malachite dye will cationic in nature which favor the nice adsorption and interaction between the oppositely charged ends. Time-dependent study was carried out in UV conditions as shown in figure-6A and in room light conditions as shown in figure-6B. Gradual change of the absorbance with time of the dye solution confirmed the presence of dye removal activity of the Fe_3O_4 NPs. Investigation of the result shows that the gradual removal of dye was observed in absorbance Vs wavelength curve up to 270 min under uv-irradiation condition distinctly in figure-6A but only few removal was observed in absorbance Vs wavelength curve up to 180 min under room light condition after that no change of UV-curve was observed up to 270min in figure-6B. Upon evaluating the outcome of the study and using equation (7) mentioned above, it was found to have 93% removal capacity (η) in UV light conditions. Besides, only 55% removal capacity (η) was found in room light conditions after 270 min. Thus, our synthesized Fe_3O_4 NPs has excellent dye removal capacity under UV light condition and it is expected that our synthesized Fe_3O_4 NPs could be suitable alternatives of other adsorbents for industrial use.

4. Conclusion

In summary, this article proposed for the first time optimum conditions to synthesize Fe_3O_4 NPs synthesis using *T. indica* leaf extract as a reductant. PBS buffer (64 mM), pH 7.4, 0.053 g/mL leaves extract concentration, and only 30 min reaction time were optimal conditions for the synthesis of Fe_3O_4 NPs. Characterization analysis confirmed its cubic morphology and particle size of 80 ± 3 nm. In XRD spectra, the magnetite Fe_3O_4 nanoparticles showed cubic-shaped crystallinity. As a result of optimizing conditions, it is found that

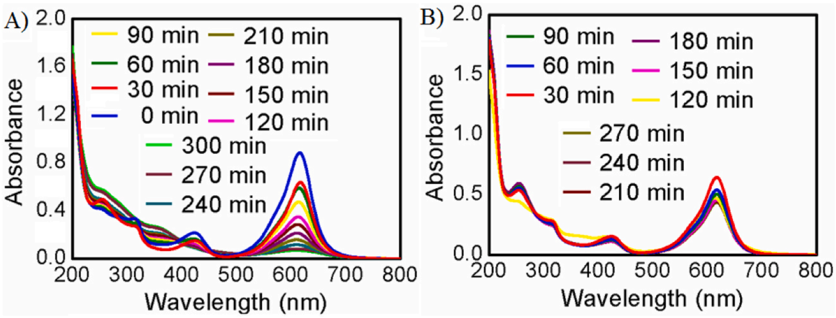

Fig. 6. UV–Visible spectra of the 10 mg/L MG in water after adding 1 mg/mL synthesized Fe_3O_4 NPs as adsorbent for a period of time in (A) UV light irradiation condition and (B) room light condition respectively.

the synthesized nanoparticles exhibited potent peroxidase activity and excellent (93%) dye removal capacity when irradiated with UV light, and good (55%) dye removal capacity when irradiated with room light. We hope that our findings from this study will have a significant impact on green nanotechnology and dye removal in industrial applications.

Author contribution statement

Md. Rajibul Akanda: Conceived and designed the experiments; Analyzed and interpreted the data; Wrote the paper.

Md. Al-amin: Performed the experiments; Analyzed and interpreted the data; Contributed reagents, materials, analysis tools or data; Wrote the paper.

Masrifa Akter Mele: Performed the experiments; Analyzed and interpreted the data; Contributed reagents, materials, analysis tools or data.

Zunayed Mahmud Shuva, Md. Billal Hossain, MD Taohedul Islam: Conceived and designed the experiments; Analyzed and interpreted the data; Contributed reagents, materials, analysis tools or data.

Md. Mehedi Hasan, Umme Habiba Ema: Analyzed and interpreted the data; Wrote the paper.

Data availability statement

Data included in article/supp. material/referenced in article.

Declaration of competing interest

The authors declare that they have no known competing financial interests or personal relationships that could have appeared to influence the work reported in this paper.

Acknowledgement

This research work was conducted by the support of Jagannath University Research grant 2021–22.

Appendix A. Supplementary data

Supplementary data to this article can be found online at https://doi.org/10.1016/j.heliyon.2023.e16699.

References

[1] J. Braunschweig, J. Bosch, R.U. Meckenstock, Iron oxide nanoparticles in geomicrobiology: from biogeochemistry to bioremediation, Nat. Biotechnol. 30 (2013) 793–802.
[2] A.K. Gupta, M. Gupta, Synthesis and surface engineering of iron oxide nanoparticles for biomedical applications, Biomaterials 26 (2005) 3995–4021.
[3] J.H. Lee, B. Schneider, E.K. Jordan, W. Liu, J.A. Frank, Synthesis of complexable fluorescent superparamagnetic iron oxide nanoparticles (FL SPIONs) and cell labeling for clinical application, Adv. Mater. 20 (2008) 2512–2516.
[4] X.-Q. Li, D.W. Elliott, W.-X. Zhang, Zero-valent iron nanoparticles for abatement of environmental pollutants: materials and engineering aspects, Crit. Rev. Solid State 31 (2006) 111–122.
[5] A. López-Serrano, R.M. Olivas, J.S. Landaluze, C. Cámara, Nanoparticles: a global vision. Characterization, separation, and quantification methods. Potential environmental and health impact, Anal. Methods 6 (2014) 38–56.
[6] F.Q. Hu, L. Wei, Z. Zhou, Y.L. Ran, Z. Li, M.Y. Gao, Preparation of biocompatible magnetite nanocrystals for in vivo magnetic resonance detection of cancer, Adv. Mater. 18 (2006) 2553–2556.

[7] H. Zhao, K. Saatchi, U.O. Hafeli, Preparation of biodegradable magnetic microspheres with poly(lactic acid)-coated magnetite, J. Magn. Magn Mater. 321 (10) (2009) 1356–1363.
[8] L. Zhang, W.F. Dong, H.B. Sun, Multifunctional superparamagnetic iron oxide nanoparticles: design, synthesis and biomedical photonic applications, Nanoscale 5 (2013) 7664–7684.
[9] A. Ali, H. Zafar, M. Zia, I. Huq, A.R. Phull, J.S. Ali, A. Hussain, Synthesis, characterization, applications, and challenges of iron oxide nanoparticles, Nanotechnol. Sci. Appl. 9 (2016) 49–67.
[10] S. Sheng-Nan, W. Chao, Z. Zan-Zan, H. Yang-Long, S.S. Venkatraman, X. Zhi-Chuan, Chin. "Magnetic iron oxide nanoparticles: synthesis and surface coating techniques for biomedical applications", Chin. Phys. B 23 (3) (2014), 037503.
[11] F. Yu, Y. Huang, A.J. Cole, V.C. Yang, The artificial peroxidase activity of magnetic iron oxide nanoparticles and its application to glucose detection, Biomaterials 30 (2009) 4716–4722.
[12] Y.A. Kurapov, E.M. Vazhnichaya, S.E. Litvin, S.M. Romanenko, G.G. Didikin, T.A. Devyatkina, Y.V. Mokliak, E.I. Oranskaya, "Physical synthesis of iron oxide nanoparticles and their biological activity in vivo", SN Appl. Sci. 1 (2019) 102.
[13] A.K. Revati, B.D. Pandey, Microbial synthesis of iron-based nanomaterials, Proc. Indian Acad. Sci. 34 (2) (2011) 191–198.
[14] R. Rasheeda, V. Meera, Synthesis of iron oxide nanoparticles coated sand by biological method and chemical method, Proc. Techn. 24 (2016) 210–216.
[15] A.V. Ramesh, D.R. Devi, S.M. Botsa, K. Basavaiah, Facile green synthesis of Fe_3O_4 nanoparticles using aqueous leaf extract of Zanthoxylum armatum DC. for efficient adsorption of methylene blue, J. Asian Ceram. Soc. 6 (2) (2018) 145–155.
[16] M. Mahdavi, F. Namvar, M.B. Ahmad, R. Mohamad, Green biosynthesis and characterization of magnetic iron oxide (Fe_3O_4) nanoparticles using seaweed (Sargassum muticum) aqueous extract, Molecules 18 (2013) 5954–5964.
[17] H. Muthukumar, M. Matheswaran, Amaranthus spinosus leaf extract mediated FeO nanoparticles: physicochemical traits, photocatalytic and antioxidant activity, ACS Sustainable Chem. Eng. 3 (12) (2015) 3149–3156.
[18] M. Bashir, S. Ali, M.A. Farrukh, Green synthesis of Fe_2O_3 nanoparticles from orange peel extract and a study of its antibacterial activity, J. Kor. Phys. Soc. 76 (2020) 848–854.
[19] H.R. Ali, Hussein N. Nassar, N. Sh El-Gendy, Green synthesis of α-Fe_2O_3 using Citrus reticulum peels extract and water decontamination from different organic pollutants, Energy Sources 39 (13) (2017) 1425–1434.
[20] D.-L. Zhao, X.-W. Zeng, Q.-S. Xia, J.-T. Tang, Preparation and coercivity and saturation magnetization dependence of inductive heating property of Fe_3O_4 nanoparticles in an alternating current magnetic field for localized hyperthermia, J. Alloys Compd. 469 (1–2) (2009) 215–218.
[21] Y.S. Kim, Y.H. Kim, Application of ferro-cobalt magnetic fluid for oil sealing, J. Magn. Magn Mater. 267 (2003) 105–110.
[22] K. Raj, R. Moskowitz, A review of damping applications of ferrofluids, Transform. Mag. 16 (2002) 358–363.
[23] D. Beydoun, R. Amal, G.K.C. Low, S. McEvoy, Novel photocatalyst: titania-coated magnetite. Activity and photodissolution, J. Phys. Chem. B 104 (2000) 4387–4396.
[24] R.D. McMicheal, R.D. Shull, L.J. Swartzendruber, L.H. Bennett, R.E. Watson, Magnetocaloric effect in superparamagnets, J. Magn. Magn Mater. 111 (1992) 29–33.
[25] L. Shen, B. Li, Y. Qiao, Fe_3O_4 nanoparticles in targeted drug/gene delivery systems, Molecules 11 (324) (2018) 1–29.
[26] Z. Gao, X. Liu, G. Deng, F. Zhou, L. Zhang, Q. Wangb, J. Lu, Fe_3O_4@mSiO_2-FA-CuS-PEG nanocomposites for magnetic resonance imaging and targeted chemo-photothermal synergistic therapy of cancer cells, Dalton Trans. 45 (2016) 13456–13465.
[27] S. Huang, C. Li, Z Cheng Y. Fan, P. Yang, C. Zhang, K. Yang, J. Lin, Magnetic Fe_3O_4@mesoporous silica composites for drug delivery and bioabsorption, J. Colloid Interface Sci. 376 (2012) 312–321.
[28] M.E. Sadat1, M.K. Baghbador, A.W. Dunn, H.P. Wagner, R.C. Ewing, J. Zhang, H. Xu, G.M. Pauletti, D.B. Mast, D. Shi, Photoluminescence and photothermal effect of Fe_3O_4 nanoparticles for medical imaging and therapy, Appl. Phys. Lett. 105 (2014) 1–5.
[29] H. Maleki-Ghaleh, E. Aghaie, A. Nadernezhad, M. Zargarzadeh, A. Khakzad, M.S. Shakeri, Y.B. Khosrowshahi, M.H. Siadati, Influence of Fe_3O_4 nanoparticles in hydroxyapatite scaffolds on proliferation of primary human fibroblast cells, J. Mater. Eng. Perform. 25 (2016) 2331–2339.
[30] P. Jiang, Y. Zhang, C. Zhu, W. Zhang, Z. Mao, C. Gao, Fe_3O_4/BSA particles induce osteogenic differentiation of mesenchymal stem cell under static magnetic field, Acta Biomater. 46 (2016) 141–150.
[31] Q.L. Jianga, S.W. Zhenga, R.Y. Hongab, S.M. Dengc, L. Guoc, R.L. Hud, B. Gaoe, M. Huange, L.F. Chenge, G.H. Liuf, Y.Q. Wangg, Folic acid-conjugated Fe_3O_4 magnetic nanoparticles for hyperthermia and MRI in vitro and in vivo, Appl. Surf. Sci. 307 (2014) 224–233.
[32] K.C. Baricka, S. Singh, D. Bahadur, M.A. Lawande, D.P. Patkar, P.A. Hassan, Carboxyl decorated Fe_3O_4 nanoparticles for MRI diagnosis and localized hyperthermia, J. Colloid Interface Sci. 418 (2014) 120–125.
[33] L.-S. Lin, Z.-X. Cong, J.-B. Cao, K.-M. Ke, Q.-L. Peng, J. Gao, H.-H. Yang, G. Liu, X. Chen, Multifunctional Fe_3O_4@polydopamine core–shell nanocomposites for intracellular mRNA detection and imaging-guided photothermal therapy, ACS Nano 8 (2014) 3876–3883.
[34] Y. Ling, K. Wei, Y. Luo, X. Gao, S. Zhong, Dual docetaxel/superparamagnetic iron oxide loaded nanoparticles for both targeting magnetic resonance imaging and cancer therapy, Biomaterials 32 (2011) 7139–7150.
[35] M.R. Akanda, U.H. Ema, M.A. Haque, M.M. Hasan, Comparative study on cupric oxide nanoparticles synthesis in saline buffer versus basic water by Spondias mombin peel extract for biocatalysis, Inorg. Nano-Met. Chem. (2022). Just accepted.
[36] M.R. Akanda, U.H. Ema, M.A. Haque, M.M. Hasan, M.A. Miah, Optimization of the cupric oxide nanoparticles synthesis by novel spondias mombin peel extract exhibited excellent peroxidase activity, J. Banglad. Acad. Sci. (2022). Just accepted.
[37] S. Kanagasubbulakshmi, K. Kadirvelu, Green synthesis of iron oxide nanoparticles using Lagenaria siceraria and evaluation of its antimicrobial activity, Def. Life Sci. J. 2 (4) (2017) 422–427.
[38] W. Ahmad, K.K. Jaiswal, M. Amjad, Euphorbia herita leaf extract as a reducing agent in a facile green synthesis of iron oxide nanoparticles and antimicrobial activity evaluation, Inorg. Nano-Met. Chem. 51 (9) (2021) 1147–1154.
[39] V.G. Kumar, A.A. Prem, Green synthesis and characterization of iron oxide nanoparticles using Phyllanthus niruri extract, Orient. J. Chem. 34 (5) (2018) 2583–2589.
[40] G. Subhashini, P. Ruban, T. Daniel, Biosynthesis and characterization of Magnetic (Fe_3O_4) Iron oxide nanoparticles from a red seaweed gracilaria edulis and its antimicrobial activity, Int. J. Adv. Sci. 3 (10) (2018) 184–189.
[41] A.V. Ramesh, D.R. Devi, S.M. Botsa, K. Basavaiah, Facile green synthesis of Fe_3O_4 nanoparticles using aqueous leaf extract of Zanthoxylum armatum DC. for efficient adsorption of methylene blue, J. Asian Ceram. Soc. 6 (2) (2018) 145–155.
[42] A. Biswas, C. Vanlalveni, R. Lalfakzuala, S. Nath, L. .Rokhum, Mikania mikrantha leaf extract mediated biogenic synthesis of magnetic iron oxide nanoparticles: characterization and its antimicrobial activity study, Mater. Today 42 (2) (2021) 1366–1373.
[43] B. Kumara, K. Smita, L. Cumbal, A. Debut, S. Galeas, V.H. Guerrero, Phytosynthesis and photocatalytic activity of magnetite (Fe_3O_4) nanoparticles using the Andean blackberry leaf, Mater. Chem. Phys. 179 (2016) 310–315.
[44] D.M.S.A. Salem, M.M. Ismail, M.A. Aly-Eldeen, Biogenic synthesis and antimicrobial potency of iron oxide (Fe_3O_4) nanoparticles using algae harvested from the Mediterranean Sea, Egypt, Egypt. J. Aquat. Res. 45 (3) (2019) 197–204.
[45] V.A. Niraimathee, V. Subha, R.S.E. Ravindran, S. Renganathan, Green synthesis of iron oxide nanoparticles from Mimosa pudica root extract, Int. J. Environ. Sustain Dev. 15 (3) (2016) 227–240.
[46] Y. Cai, Y. Shen, A. Xie, S. Li, X. Wang, Green synthesis of soya bean sprouts-mediated superparamagnetic Fe_3O_4 nanoparticles, J. Magn. Magn Mater. 322 (19) (2010) 2938–2943.
[47] M. Yusefi, K. Shameli, O. Su Yee, S.-Y. Teow, Z. Hedayatnasab, H. Jahangirian, T. J Webster, K. Kuča, Green synthesis of Fe_3O_4 nanoparticles stabilized by a Garcinia mangostana fruit peel extract for hyperthermia and anticancer activities, Int. J. Nanomed. 16 (2021) 2515–2532.
[48] M. Nasrollahzadeh, M. Ataroda, M. Sajadi, Green synthesis of the Cu/Fe_3O_4 nanoparticles using Morinda morindoides leaf aqueous extract: a highly efficient magnetically separable catalyst for the reduction of organic dyes in aqueous medium at room temperature, Appl. Surf. Sci. 364 (2016) 636–644.

[49] P. Cheera, S. Karlapudi, G. Sellola, V. Ponneri, A facile green synthesis of spherical Fe_3O_4 magnetic nanoparticles and their effect on degradation of methylene blue in aqueous solution, J. Mol. Liq. 221 (2016) 993–998.
[50] E.C. Nnadozie, P.A. Ajibade, Green synthesis and characterization of magnetite (Fe_3O_4) nanoparticles using Chromolaena odorata root extract for smart nanocomposite, Mater. Lett. 263 (2020), 127145.
[51] Y.P. Yew, K. Shameli, M. Miyake, N. Kuwano, N.B. Bt A. Khairudin, S.E.B. Mohamad, K.X. Lee, Green synthesis of magnetite (Fe_3O_4) nanoparticles using seaweed (Kappaphycus alvarezii) extract, Nanoscale Res. Lett. 11 (2016) 276.
[52] I.P. Sari, Y. Yulizar, Green synthesis of magnetite (Fe_3O_4) nanoparticles using Graptophyllum pictum leaf aqueous extract, IOP Conf. Ser. Mater. Sci. Eng. 191 (2017) 1–5.
[53] S. Venkateswarlu, Y.S. Rao, T. Balaji, B. Prathima, N.V.V. Jyothi, Biogenic synthesis of Fe_3O_4 magnetic nanoparticles using plantain peel extract, Mater. Lett. 100 (2013) 241–244.
[54] S.K. Arjaghi, M.K. Alasl, N. Sajjadi, E. Fataei, G.E. Rajaei, Green synthesis of Fe_3O_4 nanoparticles by RS Lichen extract and its application in removing heavy metals of lead and cadmium, Biol. Trace Elem. Res. 199 (2) (1999) 763–768.
[55] R.R. Koli, M.R. Phadatare, B.B. Sinhad, D.M. Sakate, A.V. Ghul, G.S. Ghodake, N.G. Deshpand, V.J. Fulari, Gram bean extract-mediated synthesis of Fe_3O_4 nanoparticles for tuning the magneto-structural properties that influence the hyperthermia performance, J. Taiwan Inst. Chem. Eng. 95 (2019) 357–368.
[56] A.A. Barzinjy, D.A. Abdul, F.H.S. Hussain, S.M. Hamad, Green synthesis of the Fe_3O_4 nanoparticles using Rhus coriaria extract: a reusable catalyst for efficient synthesis of some new 2-naphthol bis-Betti bases, Inorg. Nano-Met. Chem. 50 (8) (2020) 620–629.
[57] G. Sathishkumar, V. Logeshwaran, S. Sarathbabu, Pradeep K. Jha, M. Jeyaraj, C. Rajkuberan, N. Senthilkumar, S. Sivaramakrishnan, Green synthesis of magnetic Fe_3O_4 nanoparticles using Couroupita guianensis Aubl. fruit extract for their antibacterial and cytotoxicity activities, Artif. Cells, Nanomed. Biotechnol. 46 (2018) 589–598.
[58] P. Kuru, *Tamarindus indica* and its health-related effects, Asian Pac. J. Trop. Biomed. 4 (9) (2014) 676–681.
[59] L.-W. Change, W.-J. Yen, S.C. Huang, P.-D. Duh, Antioxidant activity of sesame coat, Food Chem. 78 (2002) 347–354.
[60] M. Chatatikun, A. Chiabchalard, Phytochemical screening and free radical scavenging activities of orange baby carrot and carrot (Daucus carota Linn.) root crude extracts, J. Chem. Pharm. 5 (4) (2013) 97–102.
[61] B. Sun, J.M. Ricardo-da-Silva, I. Spranger, Critical factors of vanillin assay for catechins and proanthocyanidins, J. Agric. Food Chem. 46 (1998) 4267–4274.
[62] Z. Kozakova, I. Kuritka, N.E. Kazantseva, V. Babayan, M. Pastorek, M. Machovsky, P. Bazant, P. Saha, The formation mechanism of iron oxide nanoparticles within the microwave-assisted solvothermal synthesis and its correlation with the structural and magnetic properties, Dalton Trans. 44 (2015), 21099.
[63] E.M. Azman, A. House, D. Charalampopoulos, A. Chatzifragkou, Effect of dehydration on phenolic compounds and antioxidant activity of blackcurrant (Ribes nigrum L.) pomace, Int. J. Food Sci. Technol. 56 (2) (2020) 1–8.
[64] L. Gao, J. Zhuang, L. Nie, J. Zhang, Y. Zhang, N. Gu, T. Wang, J. Feng, D. Yang, S. Perrett, X. Yan, Intrinsic peroxidase-like activity of ferromagnetic nanoparticles, Nat. Nanotechnol. 2 (2007) 577–583.
[65] L. Gao, J. Wu, D. Gao, Enzyme-controlled self-assembly and transformation of nanostructures in a tetramethylbenzidine/horseradish peroxidase/H2O2 system, ACS Nano 5 (2011) 6736–6742.
[66] S. Rani Sumanjit, R.K. Mahajan, Equilibrium, kinetics and thermodynamic parameters for adsorptive removal of dye Basic Blue 9 by ground nut shells and Eichhornia, Arab. J. Chem. 9 (2016) S1464–S1477.
[67] G. Sathishkumar, V. Logeshwaran, S. Sarathbabu, P.K. Jha, M. Jeyaraj, C. Rajkuberan, N. Senthilkumar, S. Sivaramakrishnan, Green synthesis of magnetic Fe_3O_4 nanoparticles using Couroupita guianensis Aubl. fruit extract for their antibacterial and cytotoxicity activities, Artif. Cells, Nanomed. Biotechnol. 46 (3) (2018) 589–598.
[68] J.K. Patra, K.-H. Baek, Green nanobiotechnology: factors affecting synthesis and characterization techniques, J. Nanomater. 417305 (2014) 12.
[69] R.D. Waldron, Infrared spectra of ferrites, Phys. Rev. 99 (6) (1955) 1727–1735.
[70] M. Ma, Y. Zhang, W. Yu, H.Y. Shen, H.G. Zhang, N. Gu, Preparation and characterization of magnetite nanoparticles coated by amino silane, Colloids Surf. A Physicochem. Eng. Asp. 212 (2–3) (2003) 219–226.
[71] Q. Li, C.W. Kartikowati, S. Horie, T. Ogi, T. Iwaki, K. Okuyama, Correlation between particle size/domain structure and magnetic properties of highly crystalline Fe_3O_4 nanoparticles, Sci. Rep. 7 (2017) 9894.
[72] P. Palladino, F. Torrini, S. Scarano, M. Minunni, 3,3′,5,5′-tetramethylbenzidine as multi-colorimetric indicator of chlorine in water in line with health guideline values, Anal. Bioanal. Chem. 412 (2020) 7861–7869.
[73] A.S. Sartape, A.M. Mandhare, V.V. Jadhav, P.D. Raut, M.A. Anuse, S.S. Kolekar, Removal of malachite green dye from aqueous solution with adsorption technique using Limonia acidissima (wood apple) shell as low cost adsorbent, Arab. J. Chem. 10 (2) (2017) S3229–S3238.